JOURNAL OF MATERIALS SCIENCE **35** (2000) 1283–1293

Fracture mechanisms of sapphire under bending

D. SHERMAN, I. BE'ERY
Department of Materials Engineering, Technion-Israel Institute of Technology, Haifa 32000, Israel
E-mail: dsherman@tx.technion.ac.il

The fracture mechanisms of a rapidly advancing crack in a single crystal are under investigation. Thin sapphire plates parallel to the basal plane were used as a model material for this purpose. Tests in three point bending (3PB) were carried out with smooth and with notched thin strip-shaped specimens having three different orientations with respect to the $(10\bar{1}0)$ plane. The effect of the orientation on the fracture mechanisms is discussed and explained.
Unique behavior was observed in the 3PB loading configuration, resulted from the typical state of stress in bending, i.e., tension in the lower, and compression in the upper region of the beam, which affected the fracture mechanisms. The continual changes of the crack direction and energy revealed a large spectrum of fracture phenomena. The major phenomena are explained. The effect of the mechanical energy on fracture mechanisms and topology is discussed.

1. Introduction

The phenomena of crack propagation in brittle materials have attracted the attention of many investigators for nearly a century. Griffith [1] established the fracture criterion for brittle materials as the critical balance between the surface energy, γ, and the mechanical energies. When the mechanical energy per unit crack advance exceeds the surface energy, unstable crack advance will result. Irwin [2] and Orowan [3] generalized the fracture criteria. When the strain energy release rate (SERR), $\mathcal{G}$, exceeds the critical fracture energy, Γ, unstable crack advance occurs, and the criterion is

$$\mathcal{G} - \Gamma = 0. \tag{1}$$

The surface energy determines the lower bound for the fracture energy $\Gamma \geq 2\gamma$. For ideally brittle materials the lower bound holds for the fracture energy, but for an advancing brittle crack, Equation 1 no longer holds, since the SERR increases with the instantaneous crack length (proportionally to the initial flaw size), whereas Γ remains nearly unchanged. Hence unbalanced energy exists in the system. Mott [4], in an attempt to explain the role of the unbalanced energy, suggested that it converts into kinetic energy, U_{K}, which obeys

$$\mathcal{G} - \Gamma = \frac{\partial U_{\mathrm{K}}}{\partial a}. \tag{2}$$

and is responsible for crack acceleration. In the first stage, the growth rate of the unbalanced energy is low, and the crack accelerates. At a characteristic terminal crack tip velocity [5–7], the kinetic energy reaches a threshold, while the mechanical energy increases. From the stress analysis point of view, Yoffe [8] has shown that the stress field in the vicinity of a running crack tip changes with the velocity and that the velocity reaches a steady state that is a certain fraction of the stress wave velocity in the solid. Feinberg *et al.* [9], measuring the crack velocity in polymethylmethacrylate (PMMA), have found velocity oscillations that coincided with the jagged structure of the fracture surface. They have also measured the terminal velocity, and found it considerably lower than that predicted by Yoffe. Extensive discussions of the phenomena of dynamic fracture of brittle solids are available [10–12].

Phenomenological observations in many classes of materials have shown that, as a crack rapidly advances or, alternatively, as the unbalanced energy increases in a brittle solid, an almost universal route of instability features the following sequence: mirror, mist, hackle and Branching [5, 13–15]. Mirror reflects a low velocity or low energy process, with no visible surface perturbations. Mist is a very small amplitude surface perturbation that leads to rougher, hackle zone, generated for cracks having high speed and almost no acceleration (terminal velocity), or, in other words, where the unbalanced energy is large. If the unbalanced energy continues to grow, branching may take place, in which the crack tip bifurcates to absorb the growing energy [5, 16]. A detailed study of the surface [7, 17–19] has indicated a close similarity between the macroscale perturbations, i.e., branches, hackle, and mist, and the nano-scale mirror perturbations. The basic feature of the perturbation consists of a crack tilting out of the main plane together with the formation of steps and filaments on its sides. The tilted crack recombines with the main crack after a distance that depends on the material, the load configuration, the excess energy, and the amplitude of the stress wave that initiates the perturbation.

It is still unclear whether the tilting element is created by the simultaneous formation of two opposing steps on the crack front [17, 18] or by splitting the crack front into fingers with an angle between them [19].

Weiderhorn [20] measured the fracture surface energies of various fracture planes and obtained significant differences: the fracture energy for the basal plane was estimated to be more than 40 $J\,m^{-2}$ but measured to be only 7.3 and 6 $J\,m^{-2}$ for $(10\bar{1}0)$ and $(\bar{1}012)$ cleavage planes, respectively. Although the stress field of the advancing crack generated high local stresses at its moving tip, no significant formation or movement of dislocations was observed, and therefore the surface energy approximately equals the fracture energy of the material. Ball and Payne [14] have reported oscillations on some fracture planes of quartz crystals. These oscillations were not stable but increased in amplitude until branching occurred. Similar results were obtained for single crystal Si by Tsai and Mecholsky [21] who also showed that the criteria for the onset of mist and hackle are the same as in amorphous materials. In discussing the problem of crack oscillation in single-crystals [10–12], it was assumed that the rationale for the oscillations is a compromise between the tendency of the crack to advance on the plane which possesses a minimum of fracture surface energy and the maximum mechanical fracture energy path associated with the K_I direction. X-ray examination of the oscillation surfaces did indeed indicate a resemblance to some favorable crack planes. The velocity measurements of branched cracks advancing on cleavage planes in single crystal Silicon, MgO, and Sapphire [5, 22] indicated that their velocities were much higher than those obtained for the same polycrystalline material.

We use sapphire as a model material to study the dynamic crack advance in a brittle single crystalline solid under bending condition, for it generates a large number of fracture mechanisms. Thin, wide and long sapphire specimens were cut from plates with surfaces parallel to the (0001) plane. The specimens were cut in three different in-plane orientations with respect to the $(10\bar{1}0)$ cleavage plane. Smooth and notched specimens were loaded to fracture. The fracture processes were identified and rationalized.

2. Experimental program

2.1. Materials

The sapphire used in this investigation has a density of 3.98 g/cm^3 (Rotem Industries, Beer-Sheva, Israel). Circular wafers of about 100 mm diameter and a nominal thickness of 0.5 mm were cut from a single crystal sapphire cylindrical block and polished. The surfaces of the wafers were parallel to the (0001) basal plane.

2.2. Specimens

The circular sapphire wafers were cut into 12 mm wide strips. Their longitudinal axis was inclined $6^\circ \pm 2^\circ$ (designated D1), $12^\circ \pm 2^\circ$ (D2) and $45^\circ \pm 2^\circ$ (D3) to the $[10\bar{1}0]$ direction, Fig. 1a, in order to gain an insight into the fracture mechanisms for different cleavage orientations. The edges of the strips were polished with a 1200 grit diamond wheel to reduce the surface flaws generated during cutting. The final geometry of the specimens was of rectangular strips of 50×10 mm^2. Some specimens were notched to determine the influence of a large pre-crack on the fracture mechanisms. Since the number of specimens was limited, no exact statistics of the failure stresses were performed.

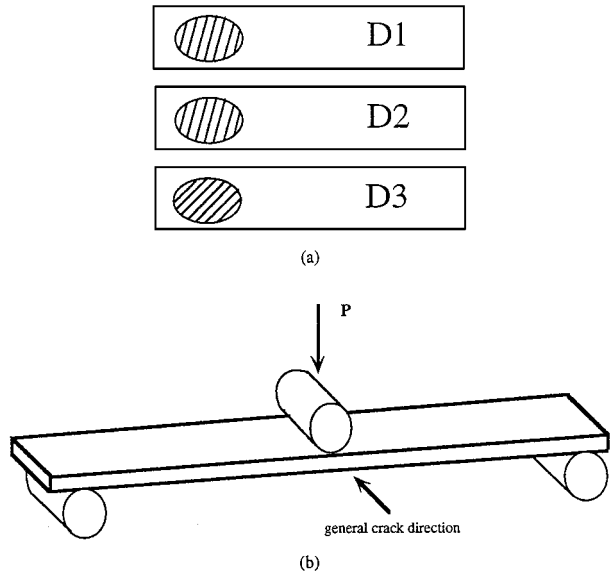

Figure 1 The orientation of the specimens with respect to the $(10\bar{1}0)$ direction (a) and the loading configuration (b).

2.3. Experimental procedure

The loading configuration was of 3PB, as shown in Fig. 1b. The specimens rested on a fully articulated 3PB fixture. The span was always 40 mm. The thickness/span ratio ensured that the maximum shear stress was less than 1 per cent of the maximum tensile stress ($\tau_{max}/\sigma_{max} = h/2L = 0.0063$).

The fracture surfaces of all the specimens were examined with optical microscope and a high resolution scanning electron microscope (HRSEM).

To gain an understanding of the advancing crack trajectory, we used Michalske and Frechette method of ultrasonic fractography [23]. A high energy ultrasonic transducer was attached to glass specimens away from the crack trajectory. The ultrasonic energy marked the advancing crack trajectory, which assisted in determining the fracture mechanisms in the sapphire specimens.

3. Results

3.1. Fracture behavior of glass under 3PB

Glass beam specimens (having the same dimensions as the sapphire specimens) were tested in the configuration depicted in Fig. 1b. The specimens behaved as a bending beam, i.e., the lower region of the cross section was initially under tension while the upper one was under compression. The Wallner lines described the propagation profile of the advancing crack after initiation, as shown in Fig. 2, and drew the crack profile until total failure occurred, as follows:

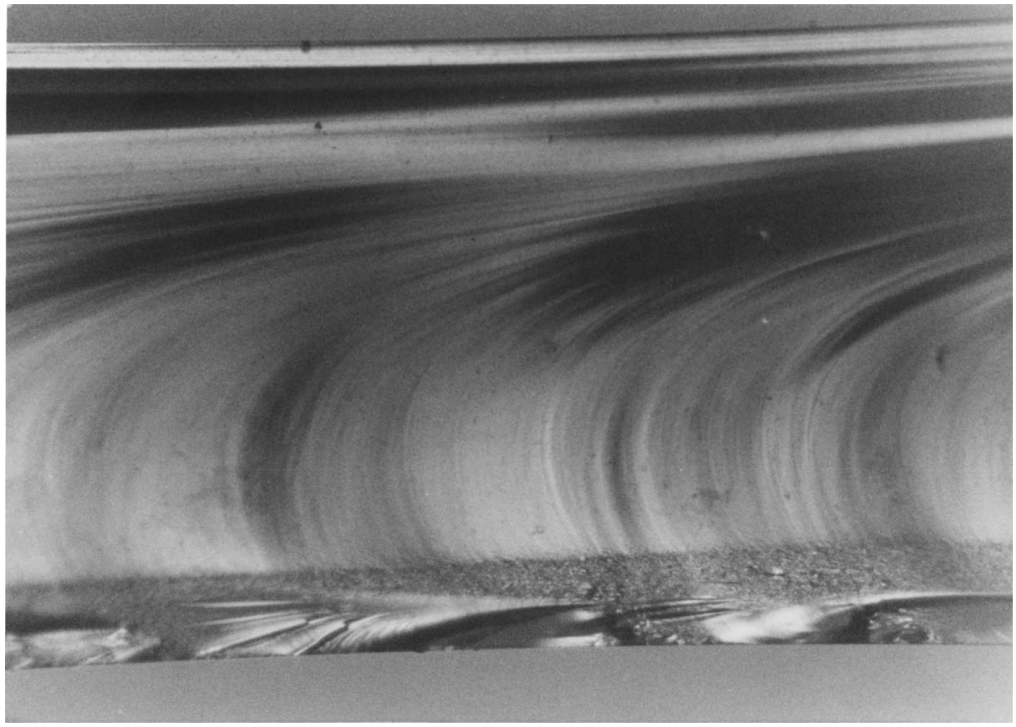

Figure 2 The Wallner lines in a glass specimen under 3PB.

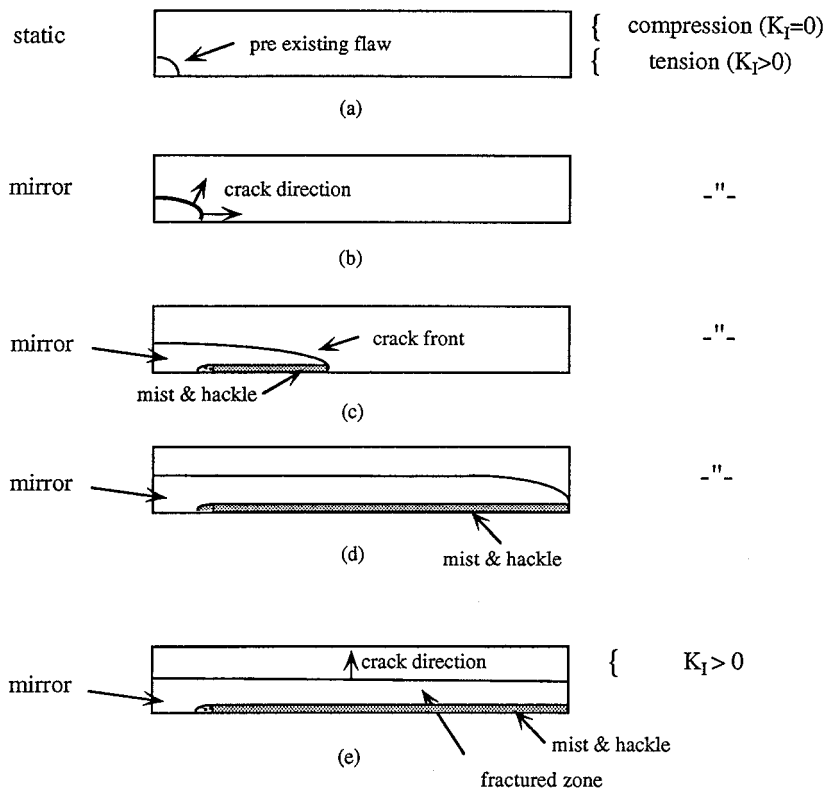

Figure 3 Schematic presentation of the advancing crack in a glass specimen. Initiation as a corner crack (a), propagation as a quarter elliptical crack in mirror profile (b), mirror and hackle for the further advanced crack (c), the crack approaching the edge of the specimen (d) changing the direction of the crack's advance (e).

i) The crack initiated as a corner crack in the lower portion of the beam's cross-section, obeying Griffith's energy balance criterion. The crack advanced as a mode *I* crack in a quarter elliptical pattern as shown in Fig. 3a.

ii) The crack then advanced as a tensile crack in the lower part of the beam, restrained by the upper portion, which was under compression, Fig. 3b, c. It is noted that the crack velocity vector is normal to the Wallner lines, Fig. 2. A mist-hackle zone was formed at this stage, as shown in the lower 'tensile' portion of the specimen.

iii) The crack approached the free edge of the specimen, Fig. 3d. The specimen now contained a deep

crack traversing its cross section. The length of the mist-hackle zone now covers most of the specimen's cross-section length in a stripe of nearly constant width.

iv) The crack now advances as a mode I crack in a wide notched beam, without any restraint. The crack velocity vector is almost normal to the specimen surface, Fig. 3e. At this stage the crack may again accelerate, but it does not reach the mirror-mist transition.

These experimental observations are in agreement with numerical analysis concerning the stress intensity factors in cracked plates under bending, indicating zero stress intensity factor in the region subjected to compressive stresses, and linearly increasing stress intensity factor in the direction normal to the plate surface in the region subjected to tensile stresses [24, 25].

3.2. Fracture behavior of sapphire under 3PB

The general nature of the advancing crack in sapphire is similar to that observed in glass, namely, the crack propagation is dictated by the increasing stress intensity factor at the 'tensile' zone and by the none positive stress intensity factor in the 'compressive' zone. However, detailed observations of the fracture surfaces of the sapphire specimens having different orientations with respect to the [1010] direction revealed the influence of the cleavage planes' orientation on the crack trajectory.

The D1 oriented specimens were fractured at a load of 15.4 ± 1.6 N, the D2 specimens at 17.5 ± 2.5 N, and the D3 at 35 ± 3.75 N. Since the number of specimens was limited, these figures are the averages of only three specimens for each direction. That indicate the initial strain energy stored in the specimens when fracture first occurs and the kinetic energy available to promote the fracture mechanisms of the advancing crack. We therefore distinguish between the fracture mechanisms for each orientation of the fracture surface with respect to the [1010] direction of the sapphire.

3.2.1. The D1 oriented specimens

The fracture mechanisms of the D1 sapphire specimens as obtained with an optical microscope are shown in Fig. 4a and b. The lower portions of these figures were initially under tension while the upper ones were under compression. The crack initiated as a short, low velocity mirror zone (not depicted), which transformed into a mist zone, shown in the lower portions of Fig. 4a and b. The mist perturbations transformed into a disturbance of larger amplitude as the crack front reached a lower amplitude of K_I along the crack front trajectory. A steady state of the fracture mechanisms is also shown in Fig. 4b. Three regions of perturbations were evident, looking from the bottom (tensile) to the top: small amplitude, a transitional, larger amplitude, and finally a mirror zone.

HRSEM micrographs of the macroscopic fracture surface shown in Fig. 4b, are shown in Fig. 5a–d. They describe the fracture mechanisms as it progressively advanced from the bottom of the cross section to the top. Smaller scale perturbations are now visible. The quarter elliptical crack advancing under tension was formed by large, flat surfaces, Fig. 5a, separated by a step constituted by crack movement on cleavage planes. Note the additional, lower scale perturbations on the flat surfaces. The next region, (Fig. 5b), demonstrates a set of

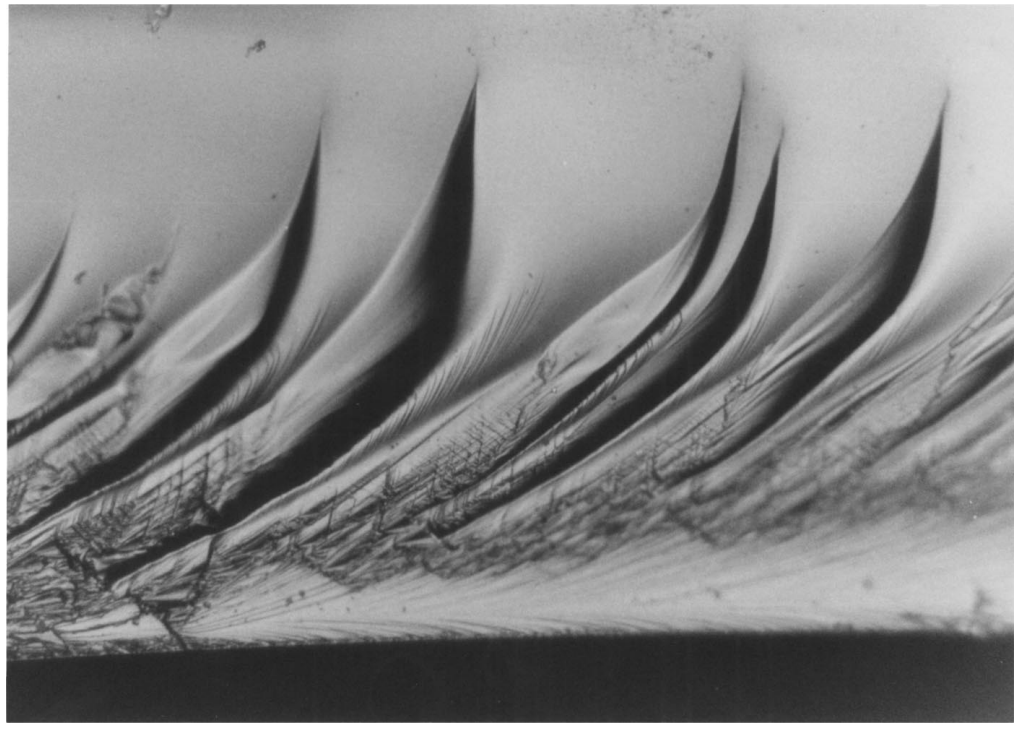

(a)

Figure 4 The initial fracture mechanisms in the D1 oriented specimen (a) (×280) and the steady state region of the fracture mechanisms (b) (×240). (*Continued*).

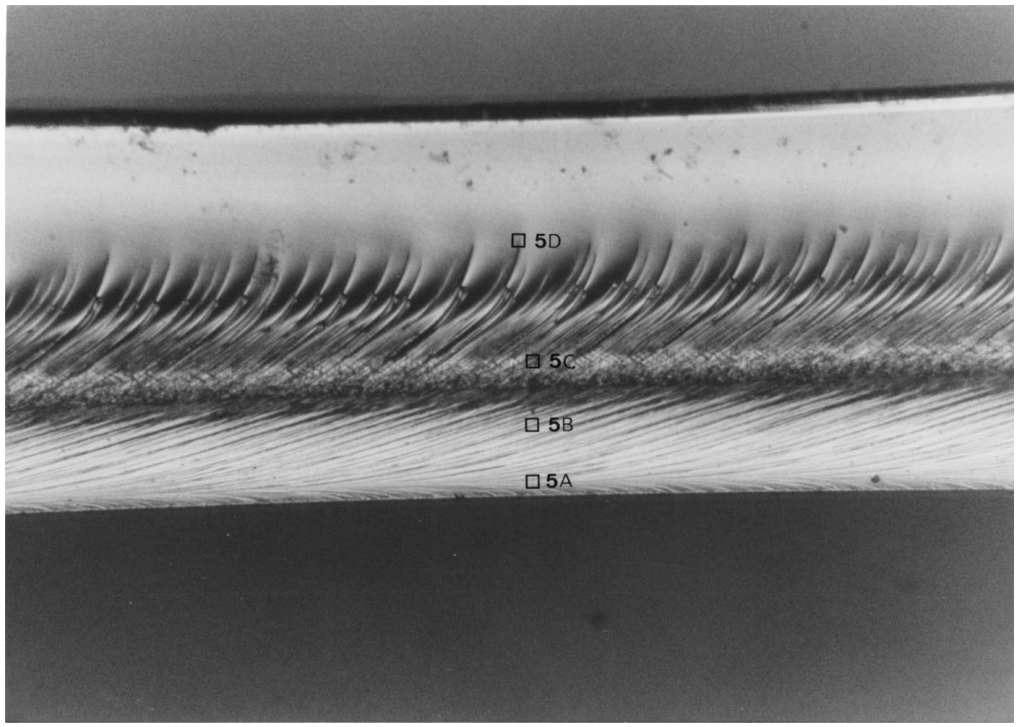

(b)

Figure 4 (*Continued*).

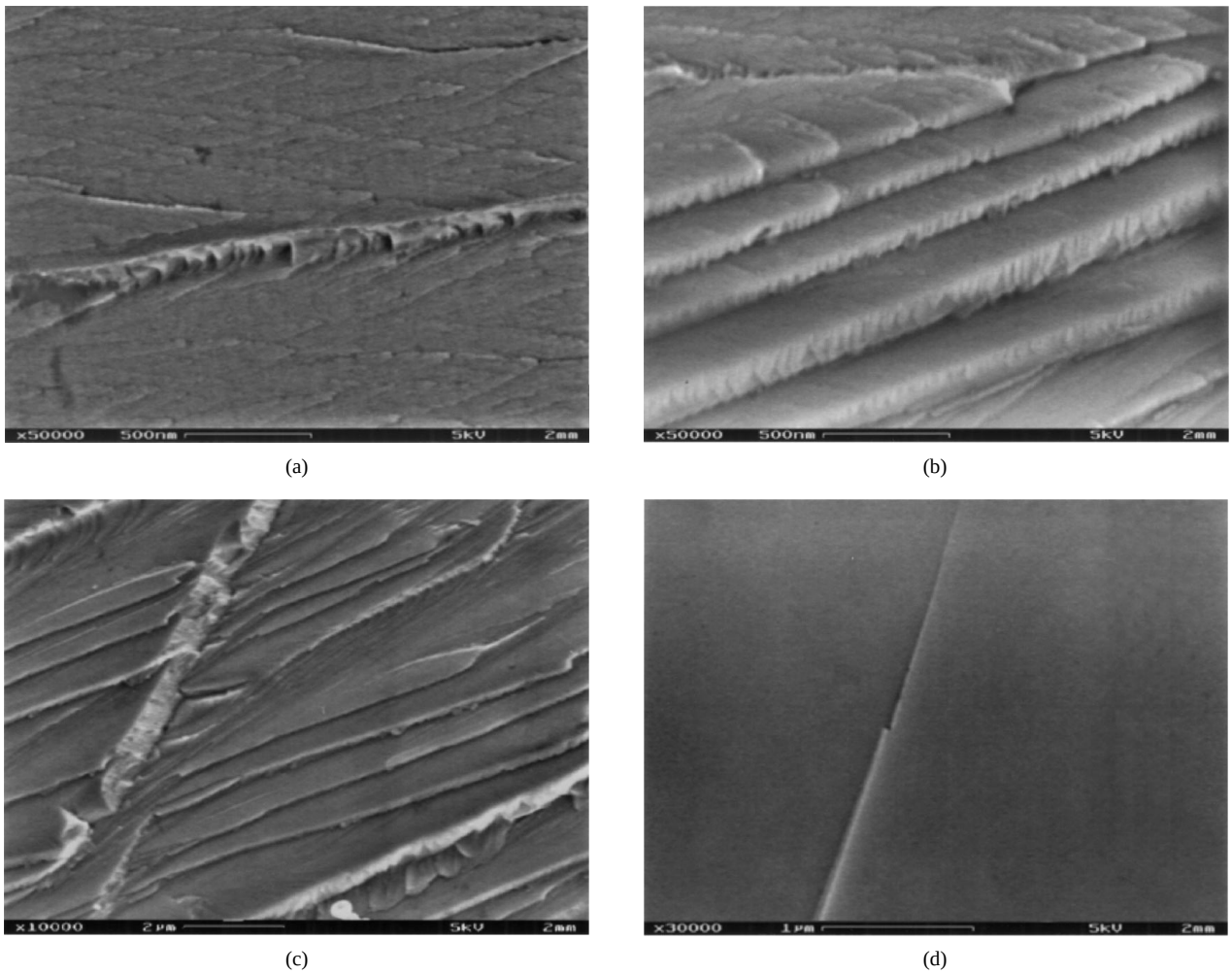

(a) (b)

(c) (d)

Figure 5 HRSEM of the fracture mechanisms of the D1 specimen. The location from which each figure was taken is shown in Fig. 4b.

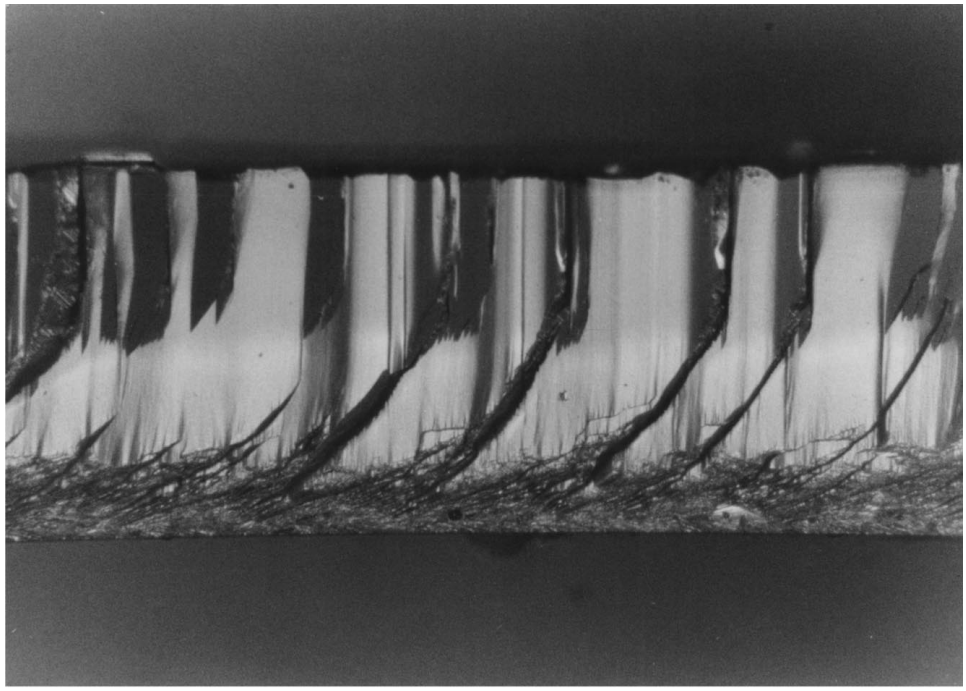

(a)

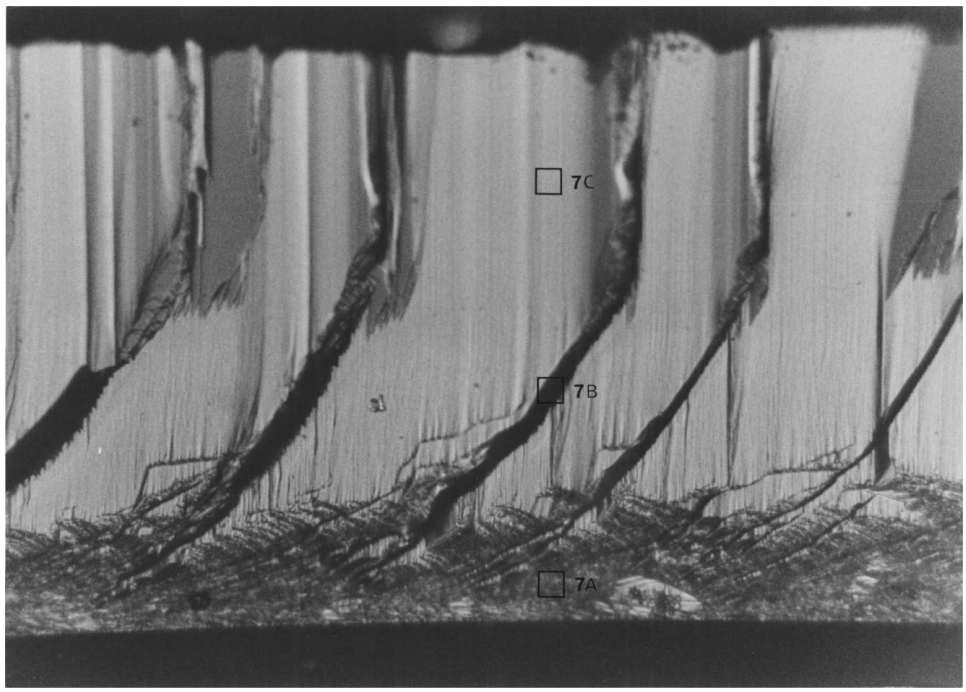

(b)

Figure 6 Optical photographs of the D2 oriented specimen at steady state (a) (×140) and at larger magnification (b) (×225).

denser, non-symmetrical steps. When the crack's velocity vector coincides with the [10$\bar{1}$0] direction, secondary perturbations of the crack surface on the {10$\bar{1}$0} cleavage planes occurred (Fig. 5c). At this stage the velocity of the semi elliptical crack decreased rapidly and the large scale perturbation vanished (Fig. 5d). The surface of the upper portion of the specimen is smooth even in a resolution of 50 nm, *although it is not a crystallographic plane*, and forms a so called mirror zone.

3.2.2. The D2 oriented specimens

The equivalent fracture surface mechanisms of these specimens obtained by an optical microscope are shown in Fig. 6a and b. The lower portion of these figures, is again, initially under tension, while the upper one is under compression. The crack initiated with a clear, low velocity mirror region that was generated under tension, followed by a very delicate mist. The fracture mechanisms at steady-state of the D2 specimen are shown in Fig. 6a and at larger magnification in Fig. 6b. In contrast to the D1 specimen, the lower part of the fracture surface revealed low amplitude high frequency perturbations over the entire specimen width. The perturbations did not decay, but continuously advanced to the top surface. On the upper surface the perturbations combine with the low surface energy cleavage planes to produce a very regular zigzag pattern. Between these regions

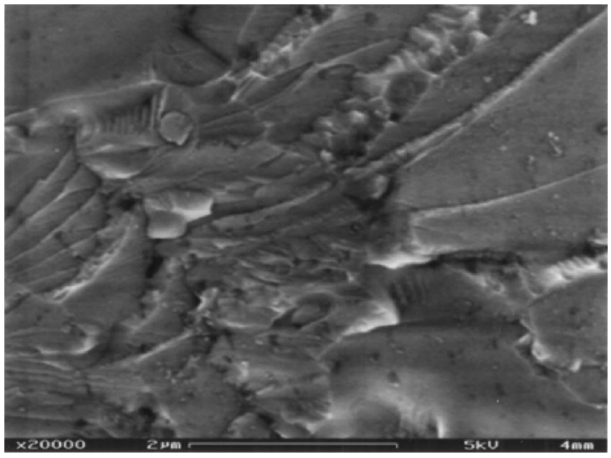

(a)

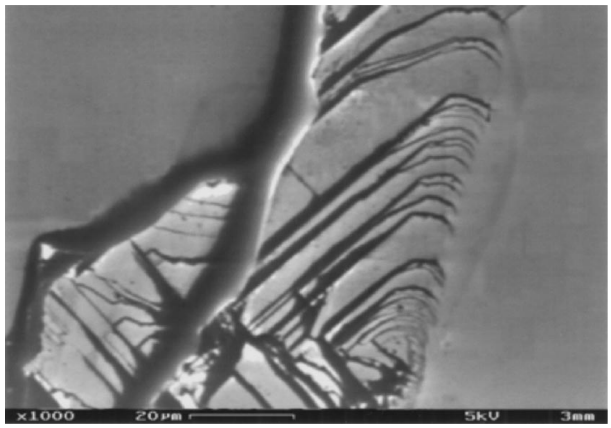

(b)

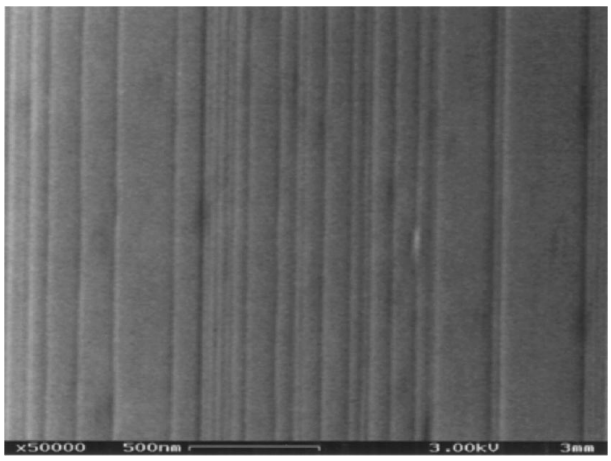

(c)

Figure 7 HRSEM of the fracture mechanisms of the D2 specimen. The location from which each figure was taken from is shown in Fig. 6a.

there is a wide transitional region with a large curved perturbation combined with smaller vertical perturbations.

HRSEM micrographs of a D2 specimen are shown in Fig. 7a–c. The perturbations in the lower portion, initially under tension (Fig. 7a), shows an unordered mixture of cleavage steps and surfaces with no visible common feature. The initiation of larger perturbations are shown in the upper-right portion of the figure. The transition from the middle region perturbations to the upper region perturbations is shown in Fig. 7b (note the scale). At this stage, the crack that moved on the mode I plane preferred to continue propagating on cleavage planes, aided by a twisting mechanism [11, 26] and resulted in a typical 'river delta' pattern. Higher magnification of the upper fracture surface, Fig. 7c, revealed very delicate parallel perturbations, 30–40 nm wide, separated by smooth cleavage planes.

3.2.3. The D3 oriented specimens

Optical photographs of these specimens were impractical due to large surface perturbations. HRSEM images are shown in Fig. 8a–d. Macroscopically, the fracture surface of these specimens was inclined $30 \pm 50^\circ$ to the (0001) direction, in agreement with the angle between the rhombohedral and the basal planes. On the other hand, the crack front direction remained close to the K_I direction, forming an angle of $30 \pm 2^\circ$ with the rhombohedral plane direction. The inclination of the crack surface caused an in plane mode I dominated mixed mode fracture. Fig. 8a is a low magnification of the fracture surface. Note the relatively smooth area in the lower (tensile) portion, large amplitude perturbations in the middle, and macroscopic fragmentation in the upper portion. The low amplitude, high frequency perturbations in the lower portion are shown in Fig. 8b. The surfaces of the large perturbations at the center of the cross section are very close to the rhombohedral $\{10\bar{1}2\}$ planes, and consisting of step like fracture mechanisms on this plane, depicted in Fig. 8c. Another phenomenon associated with the fracture of this specimen is the formation of two secondary cracks, as shown in Fig. 8d, as an additional energy absorption process.

Additional optical photographs, Fig. 9a and b, provide an additional insight into the fracture mechanisms of sapphire. The direction of this specimen lies between D1 and D2 specimens, unable to be measured unequivocally. Note the additional, many fracture mechanisms that are not included in the scope of this work. The initiation of these perturbations is very similar to that observed in the D2 specimens. Two distinct phenomena are shown: a wavy, mirror like region in the bottom portion, and a clear border line between the low amplitude high frequency perturbation and the other, high amplitude low frequency perturbation. However, the majority of the fracture processes were similar to those obtained in the D1 and the D2 specimens. An HRSEM of the high frequency region of this specimen, Fig. 9c, reveals a pattern very similar to the mist/hackle in glass [17, 18].

4. Discussion

4.1. General description of the fracture

Based on the above observations and with those obtained from the glass specimen, we deduce the following phenomenological cracking mechanisms in the sapphire:

i) The crack initiates as a corner crack in the lower portion of the beam, under maximum tensile stresses and obeying the Griffith's energy balance criterion. The crack advances as a mode I crack in a quarter elliptical pattern as shown in Fig. 10a with atomic scale perturbations (a mirror like pattern).

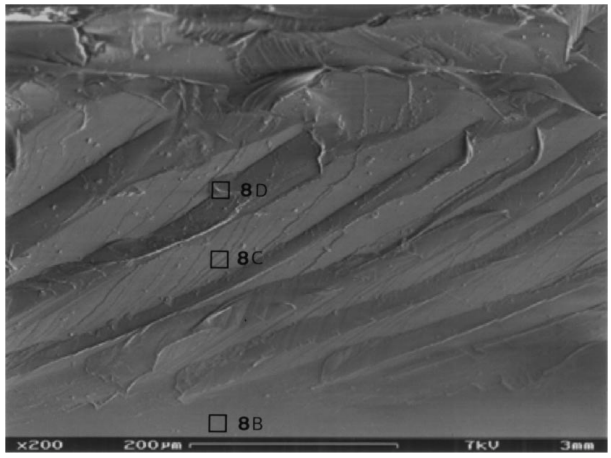

(a)

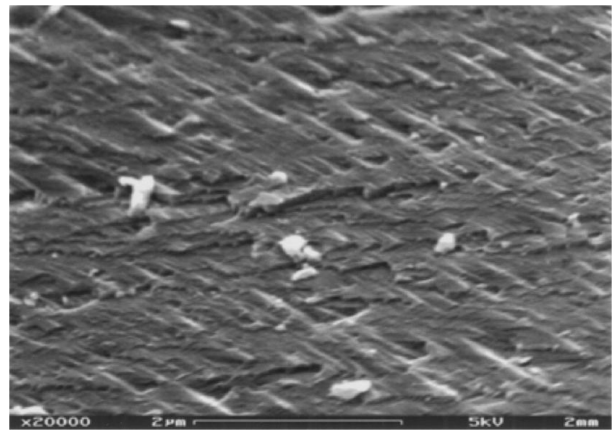

(b)

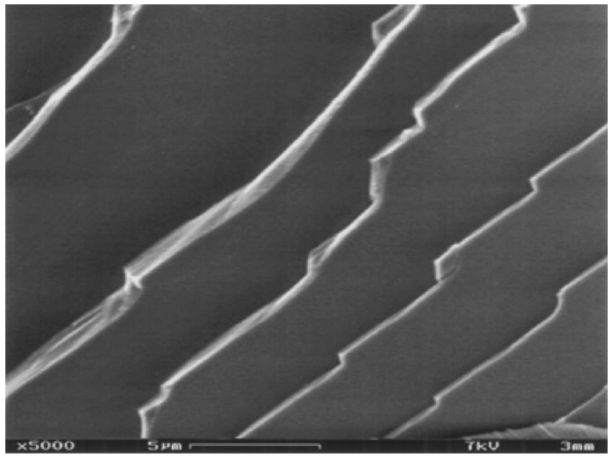

(c)

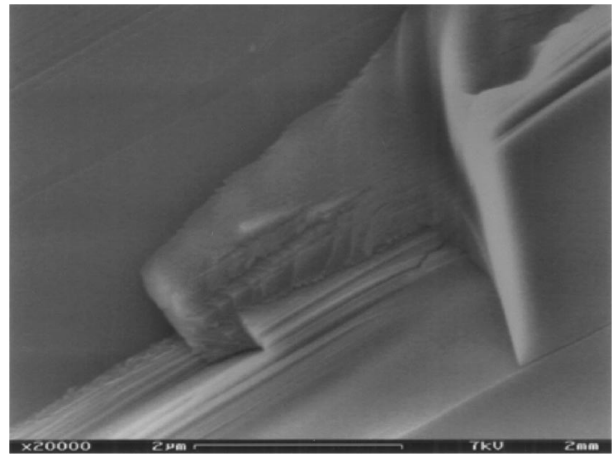

(d)

Figure 8 HRSEM micrographs of the D3 fracture surface. Low magnification (a), low amplitude, high frequency perturbations in the lower portion (b), the surfaces of the large, step like perturbations (c), and secondary cracks (d).

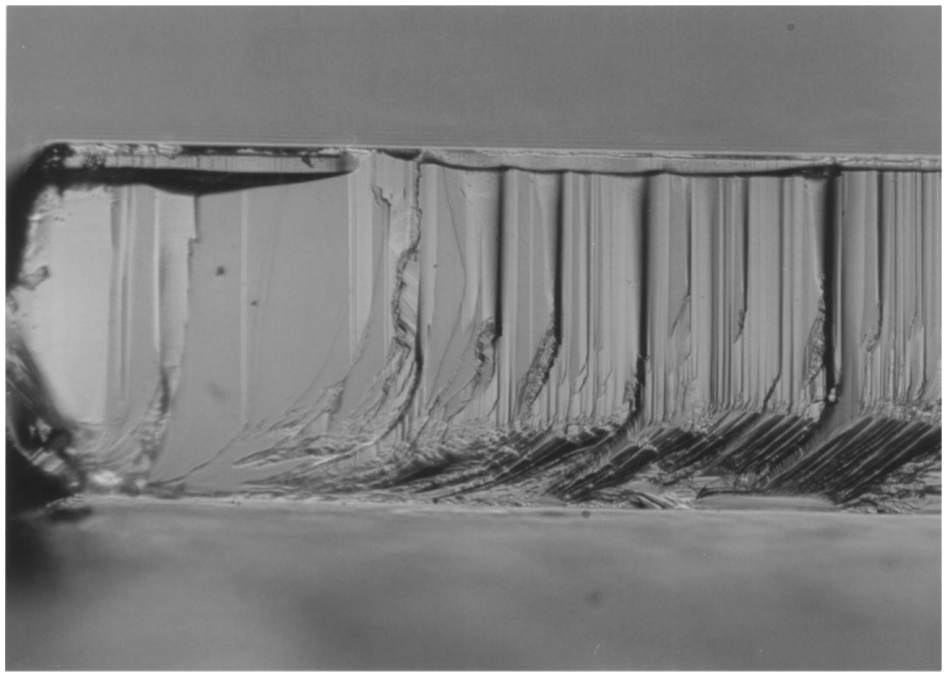

(a)

Figure 9 Optical photographs of sapphire specimen oriented between D1 and D2 directions which demonstrate the many additional fracture mechanisms (a and b) (×140), and the beginning of the steady state of the perturbations (c). (*Continued*).

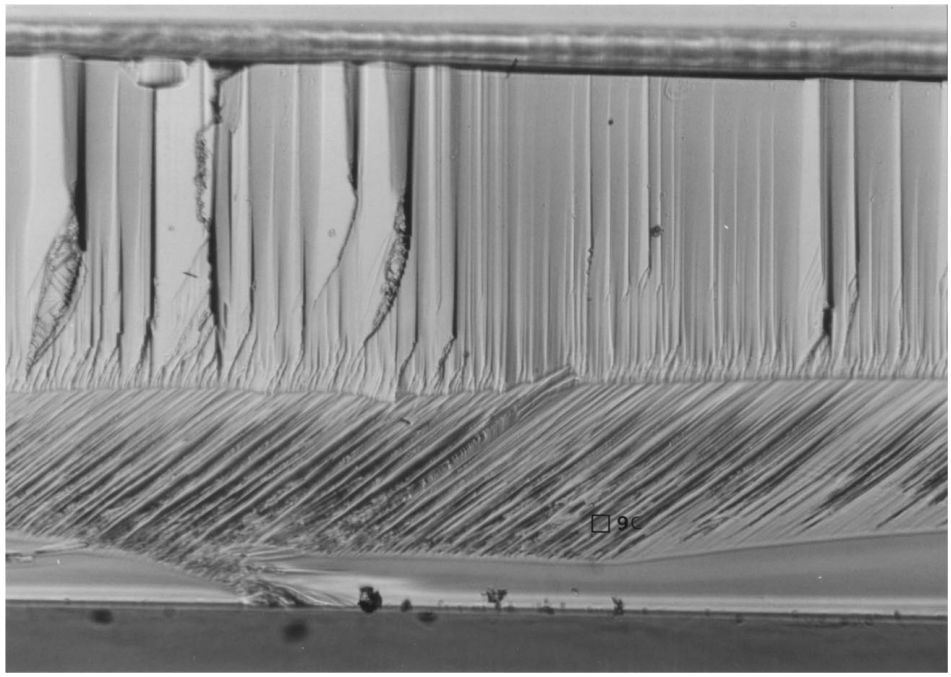

(b)

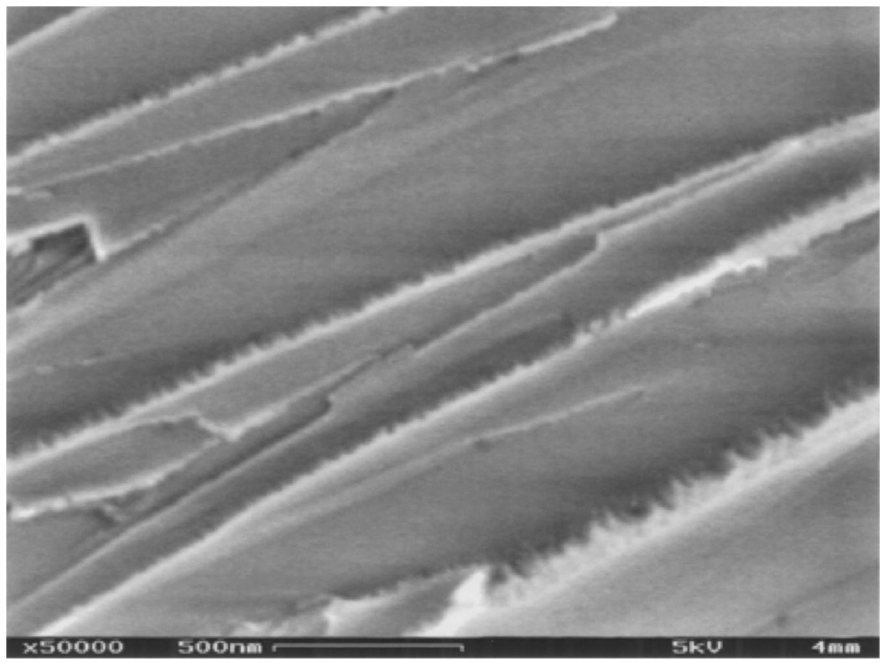

(c)

Figure 9 (*Continued*).

ii) The crack then advances as a tensile crack in the lower portion of the beam, restrained by the upper portion, which is under compression, Fig. 10b and c. The crack velocity vector is normal to the Wallner lines, as depicted in Fig. 2 for glass. A hackle zone is formed in the lower portion of the 'tensile' part of the specimen, similar to that observed in the glass specimen, but different in nature. Above this zone, a transient, larger scale zone is formed. This occurrence is in contrast to the glass specimen, Fig. 2, where only a mirror zone was observed at this location. These phenomena are associated with the preferred cleavage planes in the sapphire, discussed below, and are schematically shown in Fig. 11.

iii) The crack approaches the free edge of the specimen, Fig. 10d. The specimen now contains a crack traversing its width. The crack front has a small inclination, as shown in Fig. 10d and e. The frequencies and amplitude of the perturbation are dictated by the local velocity at the crack front.

iv) The crack now advances without any restraint. The crack velocity vector is almost normal to the specimen surface, Fig. 10e. The amplitude and the frequency of the perturbations are dictated by the previous step. For D1 specimens, the perturbation at this stage decay to form a mirror like pattern, Fig. 4b. In D2 and D3 specimens the perturbations do not completely decay, but evidence for reduced perturbations is shown in Fig. 8b.

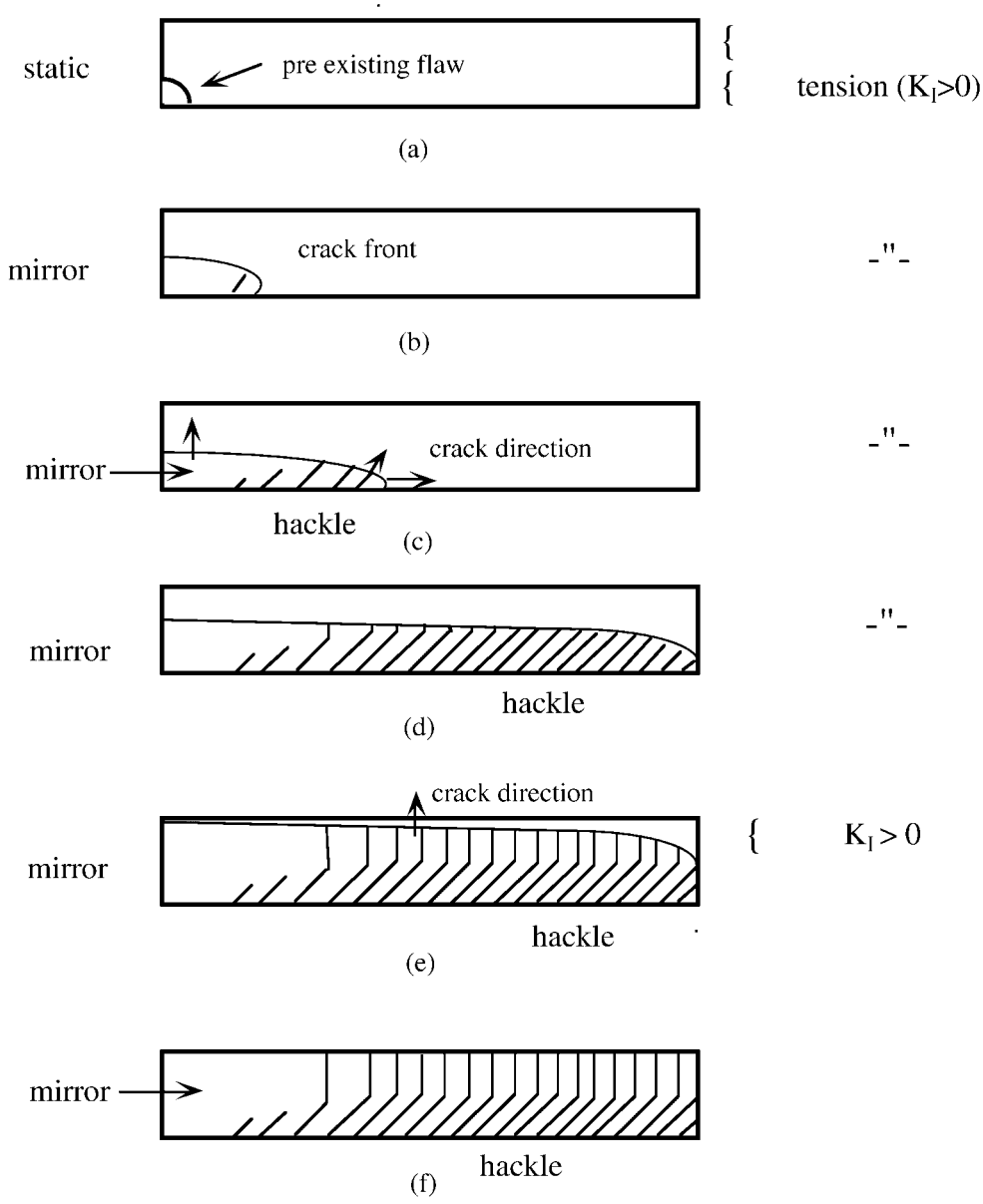

Figure 10 Schematic presentation of the advancing crack in a sapphire specimen. Initiation as a corner crack (a), propagation as a quarter elliptical crack in mirror profile (b), mirror and hackle of the advancing crack (c), the crack approaching the edge of the specimen (d), advancing with small inclination (e), and completion of the fracture mechanisms (f).

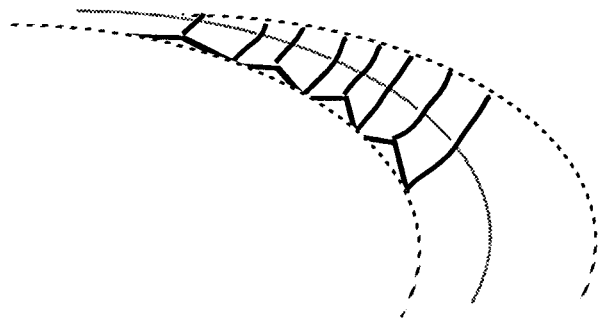

Figure 11 Schematic presentation of the spatial perturbations in sapphire, in association with Fig. 10b and c.

Introducing a notch in the specimen before loading resulted in a longer mirror region, followed by similar perturbations occurring spatially in a smooth (unnotched) specimen. It is therefore concluded that the perturbations in the upper region are a consequence of those of the lower region and are not independent phenomena. In other words, the perturbations that formed under tension initiate those fracture mechanisms in the upper portion.

As mentioned earlier, the sapphire crystal has three low energy cleavage plane families: {1010}, {1120} and {1012}. All other cleavage planes have a considerably higher surface energy, so that they may be activated only in a section subjected to a very high stress intensity factor at the crack front, and that only if no combinations of the lower energy planes are possible. If the crack front direction does not match any cleavage plane, a combination of two (or more) intersecting cleavage planes is needed.

A cross section of the crack front of a D2 oriented specimen at stage iv depicts a profile of intersecting planes with a constant angle of 150° between the planes. This implies that the crack advanced over the (1010) and (1120) cleavage planes of low fracture surface energy. In the D3 oriented specimens the cleavage planes

through most of the width are both of the $(10\bar{1}2)$ family with a typical angle of 115 ± 5, changing to $\{10\bar{1}2\}$ and $\{10\bar{1}0\}$ in the upper portion.

4.2. Energy considerations

Numerous and complicated fracture phenomena were observed and are demonstrated above. The crack front shape is dictated by the access kinetic energy rate, Equation 2, in the system. For low kinetic energy, the crack will move in the lowest energy path accessible. In a homogenous isotropic material the only path dependent term is the mechanical strain energy release rate, $\mathcal{G}$. In the case of a single crystal, the material property, Γ is also path dependent, and its influence must be taken into account.

Since $\mathcal{G}$ is a smooth function, any deflection of the crack from maximum strain energy release rate path will cause a returning force around the maximum of $\mathcal{G}$. For a pure mode I direction, which is not a crystallographic direction, the crack will always kink to a cleavage (crystallographic) plane. Consequently, the returning force is increased in magnitude. At a certain stage, the crack kinks into another cleavage plane, back to the pure mode I axis. The result is a temporal zigzag perturbation of the propagating crack front. Since the surface fracture energy of cleavage planes is constant, and since the crack area is a function of only the angle between the cleavage planes and not the amplitude of the perturbations, the overall energy, ΓA (A denotes the overall surface area of the crack) is not a function of the perturbations' amplitude. Hence, the latter is determined by the mechanical strain energy, which tends to lower the amplitude of the perturbations to a minimum. We attribute the low amplitude perturbations in the low energy case to the gradients in the stress field typical for the 3PB geometry, where the kinked crack propagates to a domain with reduced stresses, for which the strain energy release rate drops. This is the reason why the lower energy areas, when not perturbed by other causes, shows a flat surface down to a scale of less than 50 nm. Furthermore, the low energy state dictates a low velocity of the crack front, in both stage (i) and stage (iv), which enables the low amplitude, high frequency zigzag perturbations: the crack is nearly in a stable condition and low irritations are conceivable.

The high energy case is more difficult to elucidate. The mechanisms in the presence of high kinetic energy, i.e., mist and hackle are unclear even in isotropic materials. We attempt to rationalize these perturbations by adducing the growing kinetic energy, which causes high velocity and hence dynamic instability [9] of the moving crack. The rapidly moving crack will not easily kink to another low energy cleavage plane, hence the magnitude of the perturbations may increase by several orders of magnitude. The anisotropy of the surface energies can amplify (D1 specimens) or reduce (D2 and D3 specimens) the perturbations' amplitude.

5. Summary

The fracture mechanisms in sapphire, mirror, mist, and hackle were studied by loading to fracture sapphire specimens in 3PB loading configurations. Slab shaped sapphire specimens having different cleavage plane directions with respect to the longitudinal axis were studied. The trajectory of the advancing crack, typical of 3PB was explained using the Wallner lines obtained for glass specimen in the same geometry and loading configuration. The amplitude of the perturbations increased as the inclination with respect to the low energy cleavage plane was increased, the higher perturbations are attributed to the higher accessible kinetic energy in the specimen.

The low amplitude perturbations are attributed to the low mechanical energy or the low accessible kinetic energy, the maximum strain energy release rate path which applies along the pure mode I axis, and the external 3PB configuration, which generates a gradient in the stress field away from the maximum K_I path. High amplitude perturbations is attributed to the high accessible kinetic energy or high velocity of the moving crack, which is not easily kinked to an adjacent low energy cleavage plane.

Acknowledgement

We gratefully acknowledge the help of Dr. W. D. Kaplan and Ms. M. Avinon in performing the HRSEM examination.

References

1. A. A. GRIFFITH, *Phil. Trans. Roy. Soc. Lond.* **A221** (1920) 163.
2. G. R. IRWIN, Fracture of Metals, ASM Pub., 1948, p. 147.
3. E. OROWAN, *Welding Journal* **34** (1955) 157s.
4. N. F. MOTT, *Engineering* **165** (1948) 16.
5. J. E. FIELD, *Contemp. Phys.* **12** (1971) 1.
6. H. SCHARDIN, in "Fracture," edited by B. L. Averebach, D. K. Felback, G. T. Hann and D. A. Thomas (Wiley, New York, 1929).
7. E. K. BEAUCHAMP, *J. Amer. Ceram. Soc.* **78** (1995) 689.
8. E. H. YOFFE, *Phil. Mag.* **42** (1951) 739.
9. J. FINEBERG, S. P. Gross, M. Marder and H. L. Swinney, *Phys. Rev. B* **45** (1992) 5146.
10. L. B. FREUND, "Dynamic Fracture Mechanics" (Cambridge University Press, Cambridge, 1990).
11. B. LAWN, "Fracture of Brittle Solids," 2nd ed. (Cambridge Solid State Science Series, Cambridge, 1993).
12. M. F. KANNINEN and C. H. POPELAR, "Advanced Fracture Mechanics" (Oxford Engineering Science Series-15, Oxford University Press, New York, 1985).
13. R. W. RICE, in "Advances in Ceramics, 22-Fractography of Glasses and Ceramics" (1986), p. 3.
14. A. BALL and B. W. PAYNE, *J. of Mater. Sci.* **11** (1976) 731.
15. Y. L. TSAI and J. J. MECHOLSKY, Jr., *Int. J. Fracture* **57** (1992) 167.
16. D. SHERMAN, J. LEMAITRE and F. A. LECKIE, *Acta Metall. Mater.* **43** (1995) 3261.
17. D. HALL, *J. Mater. Sci.* **31** (1996) 1829.
18. *Idem., ibid.* **31** (1996) 4483.
19. D. M. KULAWANSA, L. C. JENSEN, S. C. LANGFORD and J. T. DICKINSON, *J. Mater. Res.* **9** (1994) 476.
20. S. M. WIEDERHORN, *J. Amer. Ceram. Soc.* **52** (1969) 485.
21. Y. L. TSAI and J. J. MECHOLSKY, Jr., *J. Mater. Res.* **6** (1991) 6.
22. J. H. GREENWOOD, *J. of Mater. Sci.* **6** (1971) 390.
23. T. A. MICHALSKE and V. D. FRECHETTE, *Int. J. of Fracture* **17** (1981) 251.
24. K. T. SUNDARA RAJA IYENGAR, M. V. V. MURTHY and M. N. BAPU RAO, *Int. J. Solids Struct.* **24** (1988) 683.
25. E. S. FOLIAS, *ibid.* **25** (1989) 497.
26. D. HALL, *Int. J. of Fracture* **62** (1993) 119.

Received 14 October 1997
and accepted 22 July 1999